2000-08

Performance, Control, and Simulation of the Affordable Guided Airdrop System

Williams, T.

American Institute of Aeronautics & Astronautics

Dellicker, S., Benney, R., Patel, S., Williams, T., Hewgley, C., Yakimenko, O., Howard, R., and Kaminer, I., “Performance, Control, and Simulation of the Affordable Guided

A00-37301

AIAA Modeling and Simulation Technologies Conference and Exhibit
14-17 August 2000 Denver, CO

AIAA-2000-4309

PERFORMANCE, CONTROL, AND SIMULATION OF THE AFFORDABLE GUIDED AIRDROP SYSTEM

S.Dellicker
US Army Yuma Proving Ground, Yuma, AZ
R.Benney, S.Patel
US Army SBCCOM, Natick, MA
T.Williams, C.Hewgley, O.Yakimenko[#], R.Howard, I.Kaminer
Naval Postgraduate School, Monterey, CA

Abstract

This paper addresses the development of an autonomous guidance, navigation and control system for a flat solid circular parachute. This effort is a part of the Affordable Guided Airdrop System (AGAS) that integrates a low-cost guidance and control system into fielded cargo air delivery systems. The paper describes the AGAS concept, its architecture and components. It then reviews the literature on circular parachute modeling and introduces a simplified model of a parachute. This model is used to develop and evaluate the performance of a modified bang-bang control system to steer the AGAS along a pre-specified trajectory towards a desired landing point. The synthesis of the optimal control strategy based on Pontryagin's principle of optimality is also presented. The paper is intended to be a summary of the current state of AGAS development. The paper ends with the summary of the future plans in this area.

I Introduction

The United States Air Force Science Advisory board was tasked to develop a forecast of the requirements of the most advanced air and space ideas to project the Air Force into the next century. The study, encompassing all aspects of Air Force operations, assessed a variety of technology developments critical to the Air Force mission. This study culminated in a report titled "New World Vistas, Air and Space Power for the 21st Century."[1] The study identified a critical need to improve the Point-of-Use Delivery; that is, getting the materiel where it needs to be, when it needs to be there. Airdrop is an important aspect of Point-of-Use Delivery. The report indicated that immediate improvements are needed with emphasis provided by the statement: "In the future, the problem of airdrop should be treated as seriously as the problem of bomb drop."

The first attempts to develop such systems are as old as the introduction of gliding, maneuverable parachutes.[2] However, practical systems had to wait for the development of hi-glide parachutes, especially the ram-air inflated parafoil. In 1969 the US Army defined requirements for and discussed such a cargo point delivery system.[3] None of attempts in the 70's and 80's to develop such a system were operationally acceptable, however nowadays such systems have been developed (see for example Ref.4).

These large-scale parafoil systems use a marker or beacon on the ground and ensure 99% landing accuracy in a hundred-yard circle around the beacon. Therefore, they provide the accuracy required with delivery from high altitude and large offset distances. The drawback is prohibitive cost for each pound of payload delivered. Alternate approaches were required to reduce system cost. Improved Affordable Airdrop Technologies are being evaluated by the team of the US Army and Air Force, the Naval Postgraduate School, The Boeing Company, and Vertigo, Incorporated. These efforts include the design and development of the AGAS, which incorporates a low-cost guidance, navigation, and control system into fielded cargo air delivery systems. This study focuses on evaluating the feasibility of the AGAS concept and encompasses the design and execution of a flight test program to assess dynamic response of a flat circular parachute, the design of initial guidance and control techniques, and to evaluate the feasibility of the AGAS concept.

II AGAS concept, architecture and components

AGAS is being evaluated as a low-cost alternative for meeting the military's requirements for precision airdrop.[5,6] Designed to bridge the gap between expensive high glide parafoil systems and uncontrolled (ballistic) round parachutes, the AGAS concept offers the benefits of high altitude parachute releases but cannot provide the same level of offset from the desired impact point (IP) as high-glide systems. The design goal of the

---

[#]: National Research Council Senior Research Associate at the NPS.

AGAS development is to provide a Guidance, Navigation, and Control (GNC) system that can be placed in-line with existing fielded cargo parachute systems (G-12 and G-11) and standard delivery containers (A-22). The system is required to provide an accuracy of 100*m*, Circular Error Probable (CEP), with a desired goal of 50*m* CEP. No changes to the parachute or cargo system are allowed.

The current design concept includes implementation of commercial Global Positioning System (GPS) receiver and a heading reference as the navigation sensors, a guidance computer to determine and activate the desired control input, and the application of Pneumatic Muscle Actuators (PMAs) to effect the control. The navigation system and guidance computer will be secured to existing container delivery system while the PMAs would be attached to each of four parachute risers and to the container (Figure 1). Control is affected by lengthening a single or two adjacent actuators. The parachute deforms creating an unsymmetrical shape, essentially shifting the center of pressure, and providing a drive or slip condition. Upon deployment of the system from the aircraft, the guidance computer would steer the system along a pre-planned trajectory. This concept relies on the sufficient control authority to be produced to overcome errors in wind estimation and the point of release of the system from the aircraft. Following subsections discuss main AGAS components.

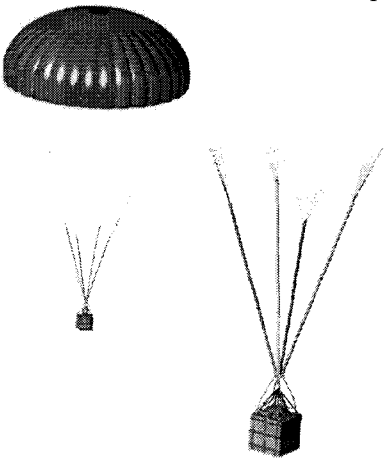

Figure 1. Affordable Guided Airdrop System#

For an airdrop mission, the aircrew will determine the Computed Air Release Point (CARP) based on the best wind estimate available at that time. The aircraft will then be navigated to that point for air delivery of the materiel. Should the wind estimate and calculation of the predicted release point be perfect and the aircrew gets the aircraft to the precise release point, then the parachute would fly precisely to the target without control inputs. However, wind estimation is far from a precise science. The calculation of the CARP relies on less than perfect estimates of parachute aerodynamics and the flight crews cannot possible precisely hit the predicted release point for each airdrop mission. Therefore, the AGAS control system design must help overcome these potential errors.

II.1 Parachute

Until now two solid flat circular parachutes C-9 and G-12 were modeled to demonstrate a feasibility of AGAS concept. (A flat circular parachute is one that when laid out on the ground forms a circle.[2]) Figure 2 shows a deployed configuration of C-9. Although the C-9 was initially designed as an ejection seat parachute, it is a standard flat circular parachute as are the larger G-11 and G-12 cargo parachutes on which AGAS will ultimately be used. Some data on these parachutes can be found in the Table 1.

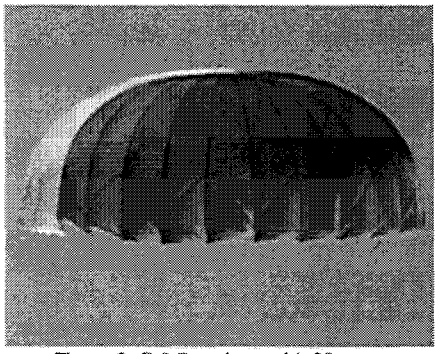

Figure 2. C-9 Parachute with 28 gores

Table 1. Parachutes data[2]

Parameter	C-9	G-12	G11-A
d_0 (ft)	28	64	100
d_P / d_0	0.67	0.67	0.67
Number of suspension lines	28	64	120
l_0 / d_0	0.82	0.80	0.90
C_{D0}	0.68	0.73	0.68
Parachute weight (lbs.)	11.3	130	215
Payload weight (lbs.)	200	2,200	3,500
Rate of descent (fps)	20	28	22

In this table d_0 denotes the nominal diameter of the parachute, d_P - inflated canopy diameter, C_{D0} - a drag coefficient, and l_0 - a suspension line length.

A cargo box is suspended from the system and houses the remote control system, control actuators, and instrumentation system.

II.2 Actuators

Vertigo, Incorporated developed PMAs[7] to effect the control inputs for this system. The PMAs are braided fiber tubes with neoprene inner sleeves that can be pressurized. Uninflated PMAs as installed on a scaled sys-

Courtesy of Vertigo, Inc., Lake Elsinore, CA.

tem are shown in Figure 3. Upon pressurization, the PMAs contract in length and expand in diameter.

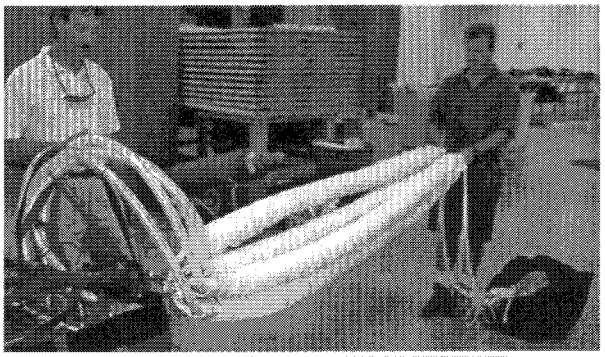

Figure 3. Pneumatic muscle actuators

With four independently controlled actuators, two of which can be activated simultaneously, eight different control inputs can be affected. The concept employed for the AGAS is to fully pressurize all actuators upon successful deployment of the parachute. To affect control of the system, one or two actuators are depressurized. This action "deforms" the parachute creating drive in the opposite direction of the control action.

Figure 4 shows a diagram of the actuator setup in the parachute payload provided by Vertigo, Incorporated, the makers of the PMAs. The gas for filling the actuators comes from 4500*psi* reservoirs (the diagram shows two, but in the simulation for this study, only a single 4500*psi* reservoir is used). Each of the four actuators are then connected to this same reservoir of nitrogen gas through some piping or tubing leading to a fill valve. The fill valve is opened to allow gas to fill the actuators when a command to take an actuation off is received. When the pressure inside the PMA reaches a certain value, a pressure switch signals the fill valve to close.

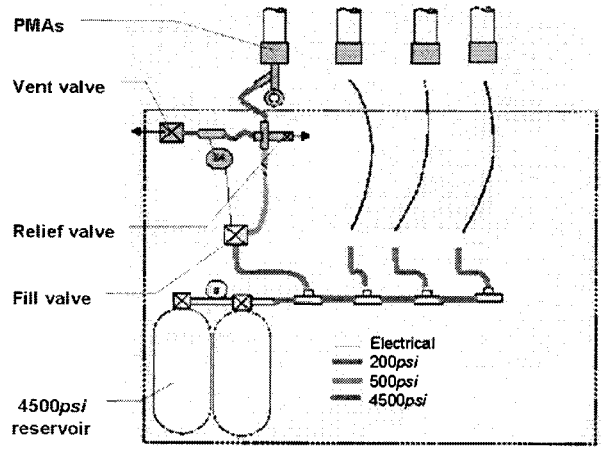

Figure 4. Vertigo, Inc. actuator system concept

Since the fill valve works with high-pressure gas it has a small orifice and therefore opens and closes rather quickly upon receiving the correct electrical signal. The time to open and close the valve is roughly 100*ms*. However, the decrease in pressure of the gas tank as more and more fills are completed slows down the actual filling process. Some of this data is plotted in Figure 5, showing increasing fill time as a function of decreasing tank pressure for actuators being filled to three different pressures.

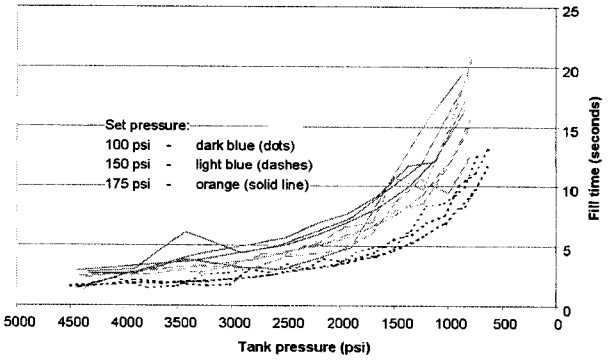

Figure 5. Fill time versus tank pressure

The vent valve opens to empty the actuator when a command to actuate is received. The vent valve has a large orifice and can open quickly to vent the PMA, but requires a certain time to vent the gas and close the orifice. The opening of the vent valve requires approximately 100*ms*, but the venting process and closing of the valve depends on the maximum pressure of the actuator fill. This process also takes a constant amount of time (approximately) because the pressure in the actuators is the same upon each vent. Figure 6 includes a diagram of the computer-modeling concept for the actuators.

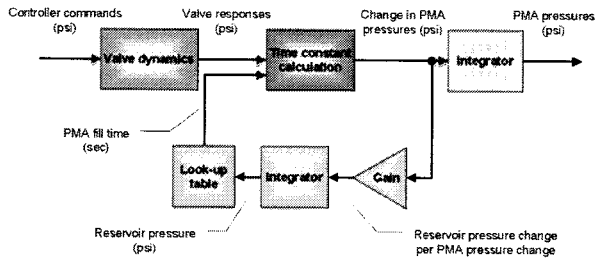

Figure 6. Actuator model

Controller commands are input to the system for each of the four PMAs. The controller commands are the pressure signals for each PMA; with 0*psi* being a vent of the actuator and 175*psi* (or the maximum pressure of the actuator) being a fill of the PMA. These commands are then passed through code that models the dynamics of the valves. This code is just a first order lag with a rise time of approximately 100*ms* to model the opening and closing of the valves. The valve responses are then passed to a code that models the actual venting and filling of the actuators, keeping in mind that the venting process takes a constant amount of time and the filling process increases with decreasing tank pressure. Once again this behavior is modeled as a first order lag. This code outputs the derivative with respect to time of the

PMA pressures. This is integrated to give the current state of each of the PMAs at a given time. PMA fill time is calculated by passing the change in PMA pressures through a gain that reflects data taken on the reservoir pressure changes per PMA pressure changes or the amount of reservoir pressure depleted for every actuator fill. This negative gain is integrated from an initial reservoir pressure to give current reservoir pressure. A look-up table is used to provide a value for the fill time of the actuators based on the remaining reservoir pressure from experimental data.

III Parachute modeling

Significant amount of research on flat circular parachute modeling has been done over past fifty years by researchers in US, Europe and Russia. It has been recognized that the basic parachute model is similar to that of a conventional aircraft. However, parachutes do have several unique features. First of all, they must be modeled as a flexible structure that includes both the parachute and the payload. Secondly, the added masses must also be modeled. And lastly it appears that no one attempted to model the control effectiveness of the risers. This section summarizes some of the research done in this area and introduces a simplified model used in this paper for preliminary analysis of control strategies.

III.1 Literature review

In 1968 White and Wolf[8] developed a 5-DOF dynamic model (ignoring the N equation, "yaw" about the downward z-axis), reviewing Henn (1944) and Lester (1962), noting that Lester discussed certain errors in the equations of motion by Henn. They noted that Lester carefully derived the equations of motion but did not attempt any solutions. They used scalar values for apparent mass and moment of inertia and conducted a dynamic stability study in which 1) steady vertical descent, 2) steady gliding ($\alpha \neq 0$, with α defined from the z axis), 3) large-angle pitch oscillation, and 4) coning are considered. A linearized analysis led to uncoupled longitudinal and lateral motions as is typical with aircraft.

It was noted that because of the shapes of the force-coefficient curves ($C_N = \sqrt{X^2 + Y^2}\left(qS_0\right)^{-1}$, the normal force coefficient, and $C_T = -Z\left(qS_0\right)^{-1}$, the tangential force coefficient), most parachutes do not fall vertically, but trim at a stable glide angle α_0. Even so, statically-stable parachutes may oscillate in pitch rather than glide. The authors noted that based on data from Heinrich and Haak[9], most parachutes could not develop sufficient $C_{N\alpha}$ to be glide stable except at high load masses, high descent rates, and low effective porosity. They noted the personnel guide surface canopy, which has low $C_{N\alpha}$ and high canopy-mass-to-payload-mass ratio, would be expected to oscillate rather than glide. Small lateral motions may result in neutrally-stable oscillations, but coning cannot develop: the longitudinal and lateral motions are uncoupled.

A nonlinear analysis produced different results. A parachute stable in the linearized sense will jump to a large-angle pitch oscillation if struck with a longitudinal disturbance greater than half of its stable angle α_0. On the other hand, a large lateral disturbance induces a longitudinal motion of comparable magnitude, throwing the parachute into a uniform vertical coning motion. To summarize: a glide-stable parachute is neutrally stable to a small lateral disturbance, but may jump into a vertical coning motion if hit with a large lateral disturbance. A single coning solution was found to exist for any given system, and only the parameters α_0 and $C_{N\alpha}$ have a great effect on coning.

Doherr[10] attempted to simulate the oscillatory behavior of a parachute and payload using two rotational DOF for the payload and three rotational DOF for the parachute. He noted that theory predicts all parachutes to assume a stable position at $\alpha = \alpha_{stable}$, while during wind-tunnel tests the less stable parachutes continued to oscillate. He recommended that aerodynamic coefficients be functions of both α and time, i.e., $C_N = C_N\left(\alpha(t), t\right)$.

Tory and Ayres[11] used a complete 6-DOF model. Differences they pointed out with White and Wolf's model are the additional DOF, forces considered on the payload, and the consideration of the apparent mass as a tensor. They showed plots of lift, drag and moment on a flat circular canopy determined from wind-tunnel tests, which will be useful for aerodynamic modeling. They modeled the apparent masses and moments of inertia based on Lamb's expressions and the assumption of the canopy being shaped as a 2:1 ellipsoid. They compared their results to some flight data, and noted that apparent inertia may not be as critical a parameter as had been suggested. A simulated drop exhibited oscillations of ±30° with a period of 5 seconds, coincident with the plane of the trajectory (therefore all pitch - no coning). Actual tests showed oscillations of 20-30° magnitude with a period of about 4-5 seconds.

Eaton and Cockrell[12] described a series of planned drop tests, from which the center of rotation was to be determined and the apparent mass estimated, but no tests were apparently conducted.

As noted by Lester and presented in the open literature by Doherr and Saliaris[13], in a 6-DOF system in which apparent mass and inertia terms are important, an apparent mass tensor can be represented by the coefficients α_{ij} to form a symmetric matrix, which for the

rigid parachute-payload system satisfies the following equalities: $\alpha_{ij} = a_{ji}$, $\alpha_{22} = \alpha_{11} \neq 0$, $\alpha_{33} \neq 0$, $\alpha_{44} = \alpha_{55} \neq 0$, $\alpha_{15} = -\alpha_{24} \neq 0$. The rest of the elements in this case are equal to zero.

Doherr and Saliaris[13] noted that predicted dynamic stability depends strongly on the math model of apparent mass. They detailed errors of Henn as pointed out by Lester. It is interesting that though White and Wolf discussed Lester's corrections of Henn's equations, they chose to use a scalar model of apparent mass and moment of inertia, rather than include the apparent-mass-tensor terms as documented by Doherr and Saliaris. Doherr and Saliaris use the set of apparent-mass terms in a small-disturbance 3-DOF model of dynamic stability. For apparent mass m_a they use half the mass of the air included within the canopy hemisphere, "arbitrarily" as noted later by Cockrell and Haidar[14]. The apparent-mass terms are given by the following equations:

$$\alpha_{11} = m_a = \frac{1}{4}\rho\frac{4}{3}\pi\left(\frac{d_P}{2}\right)^3,\ \alpha_{22} = \alpha_{11},\ \alpha_{33} = 2\alpha_{11},$$

$$\alpha_{55} = 0.048\alpha_{11}d_P^2 \text{ and } \alpha_{15} = \pm 0.2\alpha_{11}l_0. \quad (1)$$

Doherr and Saliaris considered five cases: i) $\alpha_{11} = \alpha_{33} = \alpha_{15} = \alpha_{55} = 0$ (all apparent mass terms being neglected); ii) $\alpha_{33} = \alpha_{11}$ and $\alpha_{15} = 0$ (apparent mass constant, without the coupling term); iii) $\alpha_{33} = 2\alpha_{11}$ (tangential apparent mass is twice normal apparent mass); iv-v) α_{15} is negative and positive.

The authors noted the importance of nonlinear force terms and apparent-mass effects. They referred to the Yavuz and Cockrell[15] study which showed that the apparent-mass terms are not constant, but are dependent upon the acceleration modulus (for example, $\dot{w}d_PV^{-2}$ for α_{33}).

Cockrell and Doherr[16] referred to White and Wolf as a widely accepted and employed parachute modeling method, yet lamented the lack of validation from flight test data. They aggressively pointed out that the equations of Tory and Ayres were developed incorrectly, though the particular errors were not noted. Cockrell and Doherr showed the same 3-DOF equations as Doherr and Saliaris denoting them as Lester's equations. They also listed the full 6-DOF form of the equations and referred to Eaton[17] for their derivation.

Yavuz and Cockrell[15] repeated the same 6-DOF equations as Cockrell and Doherr with the same remaining independent apparent-mass terms: α_{11}, α_{33}, α_{55}, and α_{15}. Experiments are described that allowed the authors to obtain values of the apparent mass coefficient k_{ij}, where $k_{ij} = \alpha_{ij}(\rho V_{vol})^{-1}$, and V_{vol} is the volume of the fluid displaced by the body - this case, the volume of a hemisphere. Values of k_{ij} are presented as functions of angle of attack and acceleration modulus ($\dot{V}d_PV^{-2}$). Values of k_{ij} may vary by a factor of four with acceleration modulus and the same with angle of attack. No estimations were made of practical values of acceleration moduli for dropped parachutes.

Eaton[17] noted in his paper that the complete form of the added mass tensor for a rigid axisymmetric parachute is obtained and implemented correctly for the first time. The error in Tory and Ayres is discussed as being a reversion to Henn's original faulty assumption of a real physical distinction between "included" and "apparent" mass. In Eaton's analysis, the actual masses of the canopy, rigging lines, and payload appear in the governing equations along with the four added mass components. Experiments led Eaton to run simulations with values of α_{11} to be 0.0 to 0.5 of its analogous solid-body inertial tensor component, with a baseline value of 0.2, and of α_{33} to be 0.0 to 1.0 of its analogous solid-body inertial tensor component, with a baseline value of 0.4. It is noted that the "current order-of-magnitude estimates (of α_{ij}) are very inadequate for stability studies on personnel-type, low-porosity systems."

Cockrell and Haidar[14] began the popular later approach of developing higher-order models, regarding the canopy and payload as coupled sub-systems. As for added mass effects, the authors followed Doherr and Saliaris, taking a representative value for all α_{ij}/m_a of 1.0.

Later papers continue to develop higher-order models (separate DOF for payload and canopy, ranging from 9 to 15 DOF).

Russian scientific school (Refs.18-20) proceed with the flexible structure parachute-payload and uses apparent-mass terms, obtained from the numerical simulation.

Summarizing, over a 30-year period, investigators have expressed concern over the lack of accurate dynamic modeling of apparent-mass effects, yet it appears that no studies have estimated practical values of acceleration moduli for coning, oscillating parachutes, or successfully implemented values for α_{ij} that treat them as functions of α or of acceleration module.

III.2 Simplified model

For preliminary study discussed in this paper the following simplified three-degree-of-freedom (3-DOF) model was used:

$$\dot{\vec{V}}_A = \begin{bmatrix}\dot{u}\\ \dot{v}\\ \dot{w}\end{bmatrix} = M^{-1}\left\{\frac{-qC_{D0}S_0}{V_A}\begin{bmatrix}u\\ v\\ w\end{bmatrix} + \begin{bmatrix}0\\ 0\\ mg\end{bmatrix} + \begin{bmatrix}F_x^{cont}\\ F_y^{cont}\\ 0\end{bmatrix}\right\} \quad (2)$$

where u, v, and w are the airspeed components on the axes of the body coordinate frame, α_{ii}, $i=\overline{1,3}$ are the apparent masses, m is the mass of payload and parachute assembly, q is the dynamic pressure, $S_0 = 0.25\pi d_0^2$ is a canopy surface area, g is acceleration due to gravity, and $F_{x;y}^{cont}$ are the force effect of the control actuators (in just the x and y directions). The apparent mass terms are based on the included canopy air mass m_a and are computed from the Eqns.1:

The wind speed is added to the airspeed to give groundspeed:

$$V_G = V_A + V_W \tag{3}$$

Control forces are calculated based on the pressure of the four actuators and the assumption (based on flight test data) that one control input at a time causes a 0.4 glide ratio and two control inputs at a time causes a 0.2 glide ratio. This control force is then used in the calculation of the linear accelerations of the parachute by Eqn.2, along with other parachute properties such as its mass, size, and weight, and the dynamic pressure of the atmosphere which is dependent on altitude. Linear acceleration is integrated to give airspeeds. Groundspeed is integrated to give true positions in x, y, and z coordinates of the parachute. The parachute also has a constant yaw rate ($\dot{\psi} = 0.03s^{-1}$) with small perturbations from this constant, and zero pitch and roll rates. These angular rates are integrated to give the Euler angles of the parachute, which are used to transform the coordinate axes of the parachute from the body to inertial coordinates or vice versa.

IV Derivation of the optimal control strategy

IV.1 General statement of optimization problem

Based on the AGAS concept introduced above, the optimal control problem for determination of parachute trajectories from a release point to the target point can be formulated as follows: *among all admissible trajectories that satisfy the system of differential equations, given initial and final conditions and constraints on control inputs determine the optimal trajectory that minimizes a cost function of state variables $\vec{z}$ and control inputs $\vec{u}$*

$$J = \int_{t_0}^{t_f} f_0(t, \vec{z}, \vec{u})dt \tag{4}$$

and compute the corresponding optimal control.

For the AGAS, the most suitable cost function J is the number of actuator activations. Unfortunately this cost function cannot be formulated analytically in the form given by expression (4). Therefore, we investigated other well-known integrable cost functions and used the results obtained to determine the most suitable cost function for the problem at hand.

IV.2 Application of Pontryagin's maximum principle of optimality

To determine the optimal control strategy we applied Pontryagin's principle[21] to a simplified model of parachute dynamics. This model essentially represents parachute kinematics in the horizontal plane (Figure 7):

$$\begin{aligned} \dot{x} &= u\cos\psi - v\sin\psi \\ \dot{y} &= u\sin\psi + v\cos\psi \\ \dot{\psi} &= C = const \end{aligned} \tag{5}$$

Each of four actuators in two control channels can be activated in the manner allowing the following discrete speed components in the axis of the parachute frame: $u, v \in [-V; 0; V]$. We considered these speed components as controls for the task at hand.

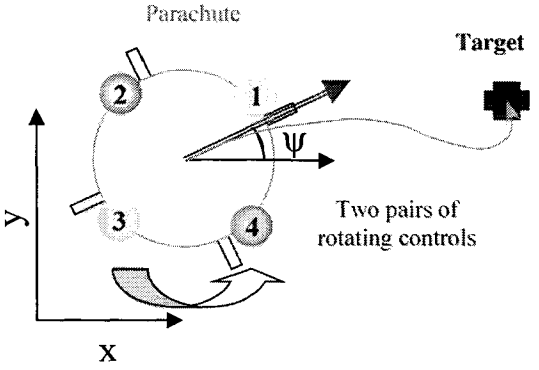

Figure 7. Projection of the optimization task onto the horizontal plane

The Hamiltonian[21] for the system (5) can be written in the following form:

$$H = (u, v)\begin{pmatrix} p_x\cos\psi + p_y\sin\psi \\ -p_x\sin\psi + p_y\cos\psi \end{pmatrix} + p_\psi C - f_0 \tag{6}$$

where equations for ajoint variables p_x, p_y, and p_ψ are given by

$$\begin{aligned} \dot{p}_x &= 0 \quad \dot{p}_y = 0 \\ \dot{p}_\psi &= (p_x, p_y)\begin{pmatrix} u\sin\psi + v\cos\psi \\ -u\cos\psi + v\sin\psi \end{pmatrix} \end{aligned} \tag{7}$$

We consider two cost functions

$$\begin{aligned} f_0 &\equiv 1 \quad \text{- minimum time} \\ f_0 &\equiv |u| + |v| \quad \text{- minimum 'fuel'} \end{aligned} \tag{8}$$

According to Ref.21, the optimal control is determined as $\vec{u}_{opt} = argmaxH(\vec{p}, \vec{z}, \vec{u})$. Therefore, for the time-minimum problem the optimal control is given by

$$u = Vsign\left((p_x, p_y)\begin{pmatrix}\cos\psi \\ \sin\psi\end{pmatrix}\right),\ v = Vsign\left((p_x, p_y)\begin{pmatrix}-\sin\psi \\ \cos\psi\end{pmatrix}\right) \tag{9}$$

Figure 8 shows the graphical interpretation of these expressions. In general, the vector (p_x, p_y) defines a

direction towards the target and establishes a semi-plane perpendicular to itself that defines the nature of control actions. Specifically, if an actuator happens to lie within a certain operating angle Δ with respect to the vector (p_x, p_y) it should be activated. For a time-optimum problem since $\Delta = \pi$ two actuators will always be active. Parachute rotation determines which two. (We do not address the case of singular control, which in general is possible if the parachute is required to satisfy a final condition for heading). Figure 9 shows an example of time-optimal trajectory. It consists of several arcs and a sequence of actuations (for this example $\dot{\psi} = 0.175 s^{-1}$ and $V = 5 m/s$).

For the 'fuel'-minimum problem we obtain analogous expression for optimal control inputs:

$$\begin{aligned} p_x \cos\psi + p_y \sin\psi > V &\Rightarrow u = V \\ p_x \cos\psi + p_y \sin\psi < V &\Rightarrow u = -V \\ p_x \cos\psi + p_y \sin\psi \equiv V &\Rightarrow u = u_{s.c.} \\ -p_x \sin\psi + p_y \cos\psi > V &\Rightarrow v = V \\ -p_x \sin\psi + p_y \cos\psi < V &\Rightarrow v = -V \\ -p_x \sin\psi + p_y \cos\psi \equiv V &\Rightarrow v = v_{s.c.} \end{aligned} \qquad (10)$$

In this case actuators will be employed when appropriate dot products will be greater than some positive value. Obviously, this narrows the value of the angle Δ. In fact, for this particular cost function $\Delta \to 0$. In general any cost function other than minimum-time will require an operating angle $\Delta \le \pi$ (Figure 10).

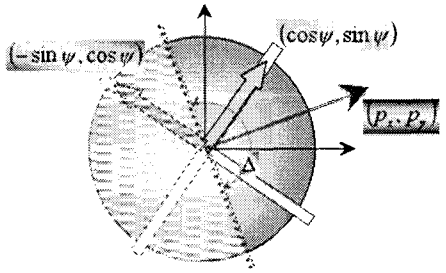

Figure 8. Time-optimal control

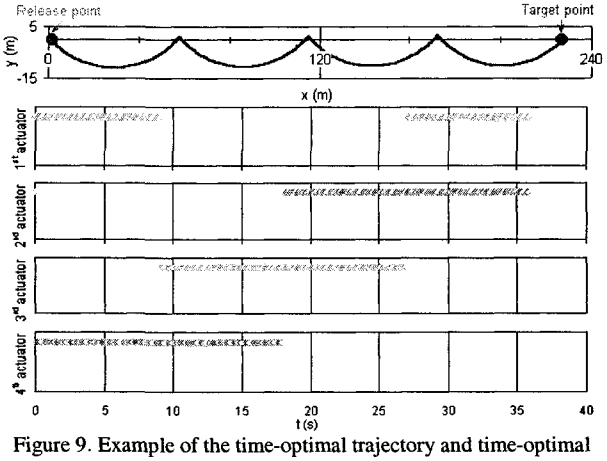

Figure 9. Example of the time-optimal trajectory and time-optimal controls

Figure 11 shows the effect of operating angle on the flight time, 'fuel' and number of actuator activations. It is clearly seen that the nature of the dependence of the number of actuations on the operating angle is the same as that of the time of flight. This implies that by solving the time minimum problem we automatically ensure a minimum number of actuations. Moreover, it is also seen that the slope of these two curves in the interval $\Delta \in [0.5\pi; \pi]$ is flat. This implies that small changes of an operation angle from its optimal value will result in negligible impact on the number of actuations. Therefore, changing the operating angle to account for the realistic actuator model will not change the number of actuations significantly.

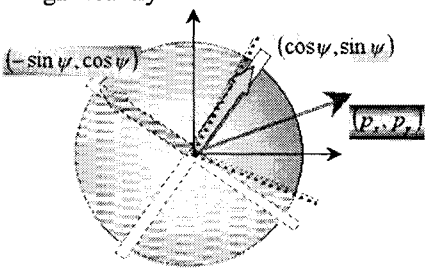

Figure 10. Generalized case of optimal control

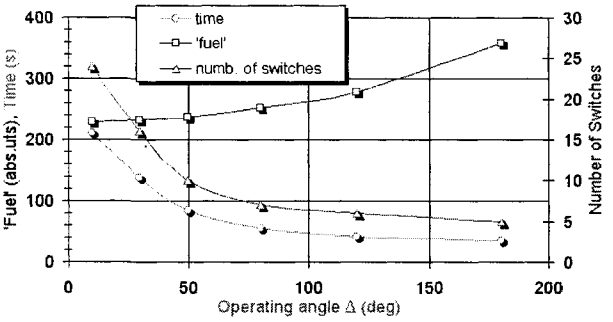

Figure 11. Influence of operating angle

IV.3 Control strategy

Preceding analysis suggested that the shape of optimal control is bang-bang. Therefore, for preliminary numerical simulation in presence of wind the control strategy was established as follows.

Considering the relatively low glide ratio demonstrated in flight test (approximately 0.4-0.5) with a descent rate of approximately $25 ft/s$[#], the AGAS could only overcome a twelve foot per second (approximately $7 kns$) wind. It is therefore imperative that the control system steers the parachute along a pre-specified trajectory obtained from most recent wind predictions. This can be done by comparing the current GPS posi-

[#] Equilibrium velocity is given by the formula $V_d = \sqrt{\frac{2mg}{C_{D0} S_0 \rho}}$, where ρ is a mass density of air at desired altitude.

tion of the parachute with the desired one at a given altitude to obtain the position error ($\vec{P}_e = \left(\vec{z}_f - \vec{z}_0\right)\Big|_{h=fix}$). Furthermore, to eliminate actuator 'oscillations', a tolerance cone is established around the planned trajectory (Figure 12) starting at 600*ft.* at the beginning of the trajectory and gradually decreasing to 60*ft.* at ground level. Should the position error be outside this tolerance, a control is activated to steer the system back to the planned trajectory. When the system is within 30*ft.* of the planned trajectory the control is disabled and the parachute drifts with the wind. Thirty feet was selected to encompass approximately one-sigma of the GPS errors (Selective Availability off).

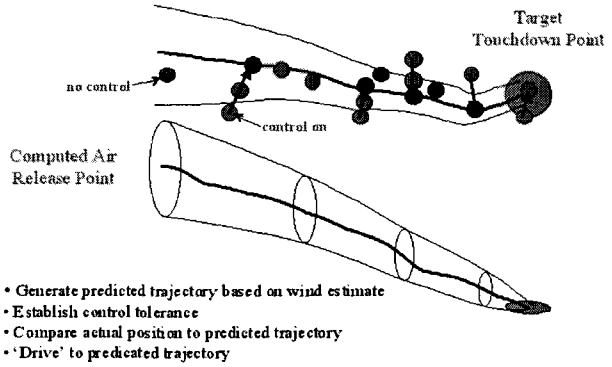

Figure 12. Control concept

As outlined above, the control system relies on the current horizontal position error to determine whether the control input is required. This position error is computed in inertial coordinate system and is then converted to the body axis using an Euler angle rotation with heading only. The resulting body-axis error (P_b) is then used to identify which control input must be activated

$$input = {}^{b}_{u}R\left(\frac{\vec{P}_e}{\left\|\vec{P}_e\right\|}\right) \tag{11}$$

Trying to account for maximum refill time and sensors errors we chose $\Delta \approx 2.5$ instead of $\Delta = \pi$ (Figure 13). This allows the activation of a single control input or two simultaneous control inputs.

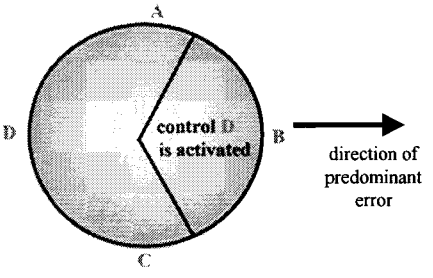

Figure 13. Control activation

Both the tolerance cone and the operating angle constraints must be active for a given PMA to be activated.

Figure 14 shows results of a simulation run that provides an insight into this control logic. The simulation uses a wind prediction profile that matches the wind profile used in the actual parachute simulation. The parachute is released at an offset from the ideal drop point of 2500*ft.* The plots show that the proper PMAs are activated (vented) when the tolerance cone and the operating angle constraints are active. One can see that at the end of the simulation that the parachute has just made it within 100*m* of the target. This brings up the concept of the "feasibility funnel." The feasibility funnel is defined as the set of points maximum distance away from the predicted trajectory for which the vehicle still has sufficient control authority to land within a certain distance from the target. The third plot in Figure 9 shows a line in the "feasibility funnel."

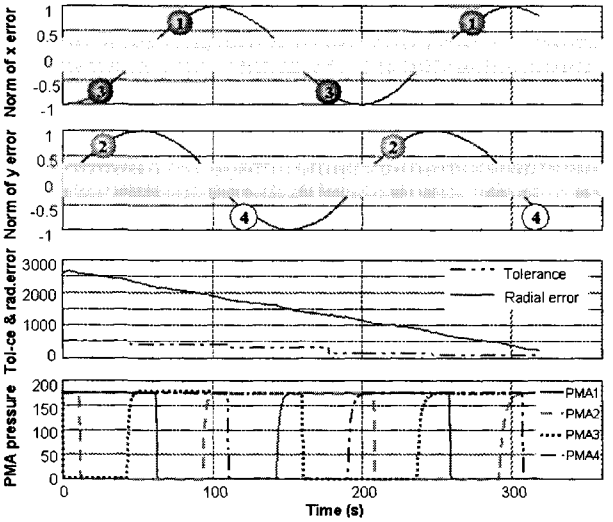

Figure 14. Example of control histories

V Simulation results

Investigation of the anticipated performance of the entire system was conducted using computer simulation incorporating the actuator model and control strategy described above. The first goal of this investigation was to determine the effectiveness of the described "trajectory-seeking" control strategy versus a control strategy that simply seeks the target landing position without using any knowledge of the winds. The second goal of this effort was to estimate the impact of changing the characteristics of the actuator system on the overall system performance.

One prerequisite to both avenues of investigation was to obtain a complete set of wind information for the drop zone. Wind information was gathered from the Yuma Proving Ground (YPG) "Tower M" drop zone using eleven Rawinsonde balloons released at one-hour intervals throughout the day on March 7th, 2000. The magnitude and direction of the wind measured by these balloons is shown in Figure 15.

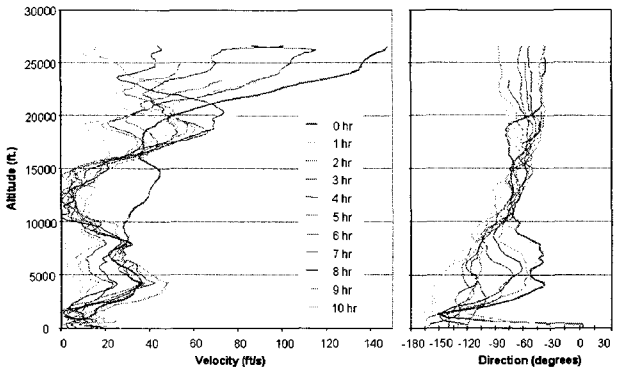

Figure 15. Measured wind velocity and direction versus altitude

In these plots, the measured wind magnitude and direction from the first balloon of the day is shown using a heavier line, and the data from the subsequent balloon releases are shown as lighter lines. Qualitative observations of wind magnitude and velocity can be gained from these plots. For the altitude range of interest, which was zero to 10,000*ft.*, the horizontal wind velocity changed by up to 20*fps* during the time span of this experiment, and wind direction in this altitude band changed by as much as 100°.

Using this wind information, a series of computer simulations of the parachute drop were conducted. The first set of simulations was run in order to visualize the effects of having a wind prediction that differs from the actual wind. The first balloon data from the day was used as a wind prediction to calculate the nominal trajectory the parachute is supposed to follow. All the subsequent balloon data were used as the actual winds, so ten actual trajectories were computed. The predicted trajectory and the ten actual trajectories are shown in a three-dimensional plot in Figure 16.

The release point of these simulated drops is directly above the origin of the horizontal plane, at an altitude of 9,500*ft.* All of the actual parachute trajectories were computed using no control of the parachute fall. The impact point (zero altitude) of the predicted trajectory has the highest positive value on the north-south axis. From the plot, it can be seen that the predicted trajectory lands north and west of the drop point, whereas the simulated drop using the last wind observation of the day lands south and west of the drop point. This observation is consistent with the wind direction data presented in Figure 16; the wind shifted from the southeast to the northeast during the course of the wind measurement experiment.

Next, a set of computer drop simulations was performed in order to assess the advantage of a control strategy that relies on a predicted trajectory based on wind information that is not current versus a control strategy that ignores the wind prediction and simply drives toward the target impact location. These two different control strategies were named "trajectory-seek" and "target-seek," respectively.

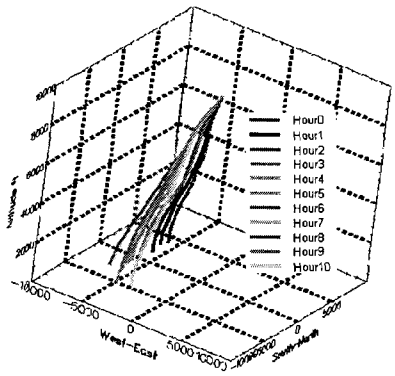

Figure 16. Sample parachute trajectories

A total of 437 simulation runs were made. On each run, the drop trajectories were computed for parachutes using both the trajectory-seek and target-seek strategies, as well as for a parachute that falls with no control inputs. Each simulation was conducted with one of the eleven Rawinsonde data files used as the actual wind for that simulation. A wind prediction was chosen at random from among the Rawinsonde data files that were gathered earlier in the day than the one selected for the actual winds. Therefore, if the data from the second balloon release of the day were chosen as the actual wind, then the data from the first balloon release of the day had to be chosen as the prediction, guaranteeing a prediction only one hour old. On the other hand, if the data from the last balloon release of the day were chosen as the actual wind, then a wind prediction from one to ten hours old could be used to compute the predicted trajectory. The predicted wind information was used in order to determine the CARP and also to determine the predicted fall trajectory for the trajectory-seek control strategy.

Another variable in these simulations was that the parachutes were dropped from a point somewhat offset from the CARP. The offset from the CARP was meant to simulate that the releasing aircraft did not hit the CARP exactly. The offsets were modeled as independent normally distributed random variables in the north-south and east-west directions. In order to determine how much of an offset to use from the CARP, an experiment was done to determine the size of the "area of attraction." This area is defined as the area around the CARP in the horizontal plane within which the parachute can be dropped and still land to within 100*m* of the target position using the onboard control system. In order to simplify this first set of experiments, the area of attraction was calculated without factoring in the effect of wind, so that the area is symmetric: a circle around the CARP in the horizontal plane. The standard deviations of the distributions of the two offsets were set at one-fourth of the radius of the area of attraction. An

overhead polar plot of the actual release and impact positions for the trajectory-seek control strategy is shown in Figure 17.

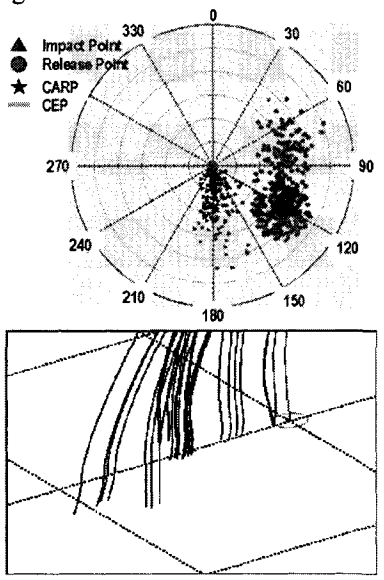

Figure 17. Trajectory-seek simulations

This plot shows that many of the release positions were southeast of the target point, relying on the predicted southeasterly winds to carry the parachute to the target point. Since the winds shifted from southeast to northeast during the day, many of the parachutes landed south of the target zone. Each of the range rings on this polar plot represents 2,000*ft*. A histogram of the simulation results is shown as Figure 18.

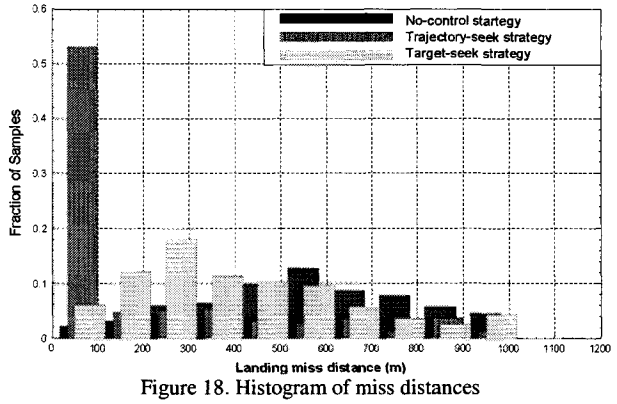

Figure 18. Histogram of miss distances

From this histogram, it can be seen that the trajectory-seek strategy showed a noticeable improvement in landing accuracy over the target-seek strategy. For the trajectory-seek strategy, over half of the simulation runs landed within 100*m* of the target, meeting the system performance goal of 100*m* of CEP. One factor affecting the data for these simulation runs was that the age of the wind predictions was not uniform. Figure 19 shows the age distribution of the wind predictions.

One can infer from this histogram that the trajectory-seek algorithm did have an advantage over the target-seek algorithm due to the fact that a substantial proportion of the simulation runs used wind data for the predicted trajectory that was fairly current.

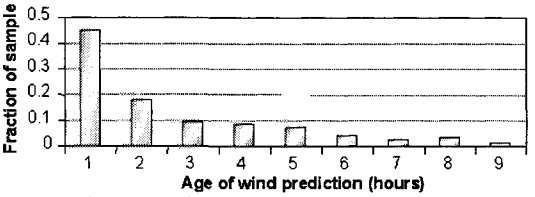

Figure 19: Distribution of wind predictions

VI Conclusions and recommendations for further research

The results presented in this paper indicate that a simple bang-bang control strategy may be sufficient to achieve the target 100*m* CEP for AGAS landing dispersion. However, further research is warranted. In particular, we propose to choose a 5-DOF model similar to the approach of White and Wolf, but with the tensor model of apparent masses and proper form of the equations from Eaton. There appears to be no current ability to resolve an accurate apparent-mass tensor as a function of anything more complex than parachute geometry. A constant yaw rate determined from flight test will be used in lieu of the 6th DOF. As a first step, the linearized 5-DOF equations will be programmed and compared to the current 2-DOF model in controlled performance. Then the nonlinear equations will be used to complete the modeling.

Aerodynamic terms will be extracted from the available terms in the literature reviewed above. Control terms will be determined from flight test data. It is of interest to estimate the relative accuracy of the current 3-DOF and the proposed 5-DOF models with regards to control strategy and required inputs. Should the added complexity of the 5-DOF model prove to contribute no apparent benefit in fidelity, the 3-DOF model will be retained.

Further analysis of the control-strategy will seek to determine the most effective operating angle Δ (because of changing aerodynamics maybe it could be better to use $\Delta \leq 0.5\pi$). Furthermore, the optimal operating angle may be asymmetric because of the different fill and vent times (Figure 21).

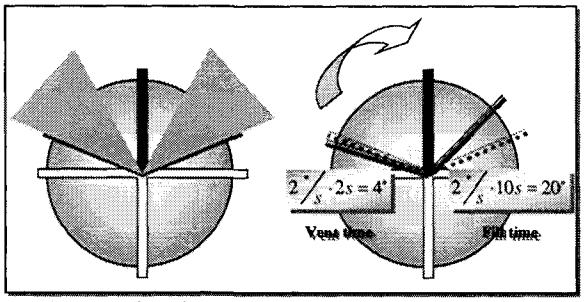

Figure 21. Questions to be answered in the further analysis

We also intend to perform additional work on determining the proper region of attraction and tolerance cone.

References

1. "Summary Report: New World Vistas, Air and Space Power for the 21st Century," United States Air Force Science Advisory Board, 1997.
2. Knacke, T.W., "Parachute Recovery Systems Design Manual," Para Publishing, Santa Barbara, CA, 1992.
3. Forehand, J.E., "The Precision Drop Dlider (PDG)," Proceedings of the Symposium on Parachute Technology and Evaluation, El Centro, CA, April 1969 (USAF report FTC-TR-64-12, pp.24-44)
4. Final Report: Development and Demonstration of a Ram-Air Parafoil Precision Guided Airdrop System, Volume 3, Draper Laboratory under Army Contract DAAK60-94-C-0041, October 1996
5. Brown, G., Haggard, R., Almassy, R., Benney, R. and Dellicker, S., "The Affordable Guided Airdrop System," AIAA 99-1742, 15th CAES/AIAA Aerodynamic Decelerator Systems Technology Conference, June 1999.
6. Dellicker, S., "Low Cost Parachute Navigation Guidance and Control," MS thesis, Naval Postgraduate School, September 1999.
7. Benney, R., Brown, G. and Stein, K., "A New Pneumatic Actuator: Its Use in Airdrop Applications," AIAA 99-1719, 15th CAES/AIAA Aerodynamic Decelerator Systems Technology Conference, June 1999.
8. White, F.M. and Wolf, D.F., "A Theory of Three-Dimensional Parachute Dynamic Stability," Journal of Aircraft, Vol.5, No.1, 1968, pp.86-92.
9. Heinrich, H.G. and Haak, E.L., "Stability and Drag of Parachutes with Varying Effective Porosity," Wright-Patterson AFB, ASD-TDR-62-100, Sept. 1962.
10. Doherr, K.-F., "Theoretical and Experimental Investigation of Parachute-Load-System Dynamic Stability," AIAA-75-1397, 1975.
11. Tory, C. and Ayres, R., "Computer Model of a Fully Deployed Parachute," Journal of Aircraft, Vol.14, No.7, 1977, pp.675-679.
12. Eaton, J.A. and Cockrell, D.J., "The Validity of the Leicester Computer Model for a Parachute with Fully-Deployed Canopy," AIAA-79-0460, 1979.
13. Doherr, K.-F. and Saliaris, C., "On the Influence of Stochastic and Acceleration Dependent Aerodynamic Forces on the Dynamic Stability of Parachutes," AIAA-81-1941, Oct. 1981.
14. Cockrell, D.J. and Haidar, N.I.A., "Influence of the Canopy-Payload Coupling on the Dynamic Stability in Pitch of a Parachute System," AIAA-93-1248, May 1993.
15. Yavus, T. and Cockrell, D.J., "Experimental Determination of Parachute Apparent Mass and Its Significance in Predicting Dynamic Stability," AIAA-81-1920, Oct. 1981.
16. Cockrell, D.J. and Doherr, K.-F., "Preliminary Consideration of Parameter Identification Analysis from Parachute Aerodynamic Flight Test Data," AIAA-81-1940, Oct. 1981.
17. Eaton, J.A., "Added Mass and the Dynamic Stability of Parachutes," Journal of Aircraft, Vol.19, No.5, 1982, pp.414-416.
18. Antonenko, A., Rysev, O., Fatyhov, F., Churkin, V. and Yurcev, Y., "Flight Dynamics of Parachute Systems," Mashinostroenie, Moscow, 1982.
19. Shevljakov, Y., Temnenko, V. and Tischenko, V., "Dynamics of Parachute Systems," Vischa Shcola, Odessa 1985.
20. Rysev, O., Belozerkovsky, S., Nisht, M. and Ponomarev, A., "Parachutes and Hang-Gliders Computer Investigations," Mashinostroenie, Moscow, 1987.
21. Pontrjagin, L., Boltjanskiy, V., Gamkrelidze, R. and Mishenko, E., "Mathematical Theory of Optimal Processes," Nayka, Moscow, 1969.